Magnetotransport phenomena in multimode lattices

Magnetotransport phenomena in multimode lattices

J Cebulski†, W Gębicki‡, V I Ivanov-Omskii§, J Polit† and E M Sheregii†

† Institute of Physics, Pedagogical University, 35-310 Rzeszów, Rejtana 16A, Poland
‡ Institute of Physics, Technical University, Warsaw, Noakowskiego 26, Poland
§ A F Ioffe Physico-Technical Institute of the Russian Academy of Science, 194021
St Petersburg, Politechnicheskaja 26, Russia

Abstract. The phonon and electron subsystems in the quaternary solid solutions of $Zn_xCd_yHg_{1-x-y}Te$ (ZMCT) were studied by means of Raman scattering and magnetophonon resonance. The Raman spectra for several compositions confirm that the phonon spectra exhibit three-mode behaviour. The cluster mode has also been observed. Four kinds of LO phonon (with HgTe-like, CdTe-like and ZnTe-like sublattices and ZnTe clusters) participate in the electron–phonon interaction. Four types of one-phonon magnetophonon resonance and two types of magnetophonon resonance on the difference of phonon frequencies have been observed. The peculiarities of the electron transport in these lattices are discussed.

1. Introduction

The scope of application of semiconductor solid solutions is constantly widening, since their material properties may be controlled (tailored) by means of composition variations. This phenomenon can be taken advantage of only on the condition that the composition variations are not accompanied by the introduction of various defects caused by lattice mismatch. In the cases of GaAs–AlAs and HgTe–CdTe solid solutions, the lattice parameters of the components are very well fitted. This leads to wide technological applicability of these materials.

Random homogeneous substitutions for matrix cations with atoms of other metals in solid-solution lattices with common anions (e.g., in the case of GaAs–AlAs or HgTe–CdTe) is known to cause a continuous reconstruction of the electronic structure and phonon spectra with composition variation. It may be assumed that the introduction of the third cation will enable us to obtain a supplementary degree of freedom in the control of the material parameters. This has an additional advantage in the case of HgTe–CdTe (MCT), because the introduction of Zn atoms stabilizes the weak Hg–Te bonds in the crystal lattice of this solid solution, whereas the presence of Cd atoms destabilizes them [1–3]. Quaternary solid solutions of $Zn_xCd_yHg_{1-x-y}Te$ (ZMCT) were first discussed by Rogalski and Piotrowski [4] (see also [5]). The state diagram and mechanical properties of ZMCT solid solutions were studied by Triboulet [2]. A series of research projects investigating the properties of this material were conducted at the A F Ioffe Physico-Technical Institute in St Petersburg [3, 6, 7]. Magnetophonon resonance, which is a powerful tool for investigation of electron and hole spectra [8], was observed in the epilayers obtained [9–11].

The introduction of the fourth component, Zn, causes not only a simple extension of the physical properties of MCT, but also new phenomena, connected with 'multimodeness'

of the crystal lattice. 'Multimodeness' is an issue of primary significance in the study of four-component solid solutions.

The phonon spectrum of HgCdTe (MCT) solid solutions is known to be characterized by two-mode behaviour [12–15]. Two other ternary solid solutions, $Zn_xCd_{1-x}Te$ (ZCT) and $Zn_xHg_{1-x}Te$ (ZMT), have two-mode phonon spectra [16–18]. The interaction of the modes in MCT results in magnetophonon resonance on the difference of phonon frequencies; this was first observed for MCT in 1988 [19].

ZMCT has three sublattices (ZnTe-like, CdTe-like and HgTe-like). Therefore, a three-mode behaviour of the phonon spectrum in this solid solution may be predicted. However, this will not necessarily be obtained [20].

The present article discusses the results of an investigation of the phonon spectra and the band structure of ZMCT. The phonon spectra of ZMCT solid solutions have been investigated by means of Raman scattering. The phonon frequencies obtained enable us to interpret the complicated structure of the magnetophonon resonance (MPR) peaks observed over a wide temperature range for three compositions of ZMCT. The peculiarities of the electron transport in a multimode crystal lattice are discussed.

Table 1. Data for the layer specimens of ZMCT.

Number of sample	x	y	Electron concentration (10^{15} cm^{-3})	Electron mobility (10^4 cm^2 V^{-1} s^{-1})
I	0.02	0.20	—	—
II	0.07	0.21	—	—
III	0.12	0.17	—	—
IV	0.08	0.11	3.5	9.0
V	0.12	0.10	5.0	5.0
VI	0.17	0.08	2.0	2.5

2. Samples

Epitaxial films of ZMCT obtained by liquid-phase epitaxy on CdTe substrates were studied. The thickness of the homogeneous layers was $d = 4$ μm. The parameters of the six ZMCT epilayers which were used in the Raman and MPR experiments are listed in table 1. The temperature dependencies of the electroconductivity and the Hall coefficient measured for samples IV–VI showed an activated behaviour. The quality of the epitaxial layers which were used in the MPR experiments (samples VI–VI) was comparable with that of the corresponding high-quality MCT alloys with the same energy gap (near 180–300 meV). The mobility of the electrons in those layers is sufficiently high for observing MPR. It is important to note that the parameters for these samples had not changed over a period of three years, whereas MCT samples are characterized by temporal degradation of their parameters.

3. Raman spectra

The Raman spectra (RS) were excited with an Ar-ion laser with power less than 200 mW and recorded with a Dilor XY spectrometer at room temperature. The laser wavelength was 514.5 nm and the spectral resolution was $\sim$4 cm^{-1}. All of the spectra were recorded in the
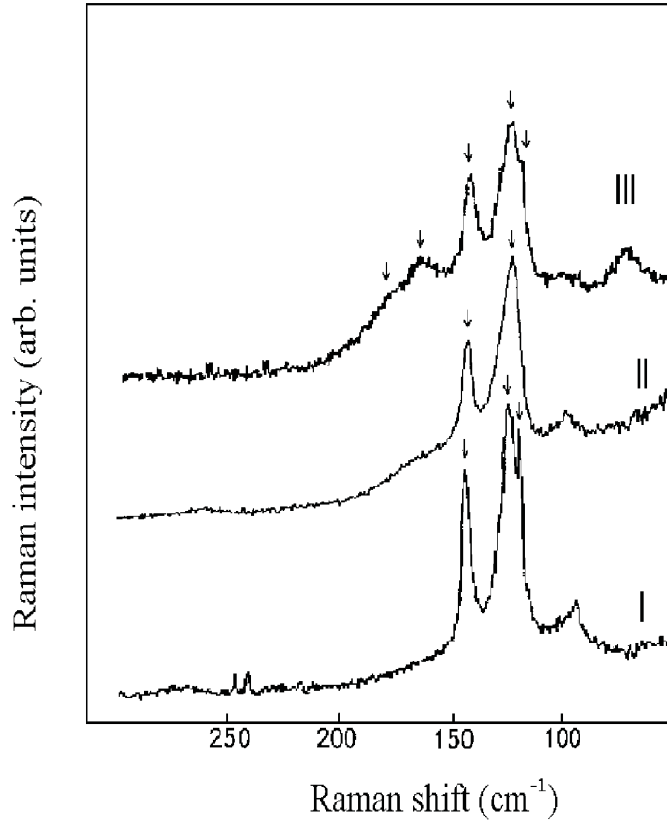
Figure 1. The Raman spectra of ZMCT solid solution at 300 K for scattering from the (111) face: curve I: sample I; curve II: sample II; and curve III: sample III. Spectral split width: 4.68 cm^{-1}.

geometry with backscattering of light from the (111) face. These experimental conditions are analogous to those for the CdTe studies in [21]. Similar measurements for MCT were taken in [22], but under slightly different conditions—namely, with polarized light.

The RS of the three samples with different amounts of ZnTe (sample I: 2% of ZnTe;

Table 2. Interpretation of the Raman spectra.

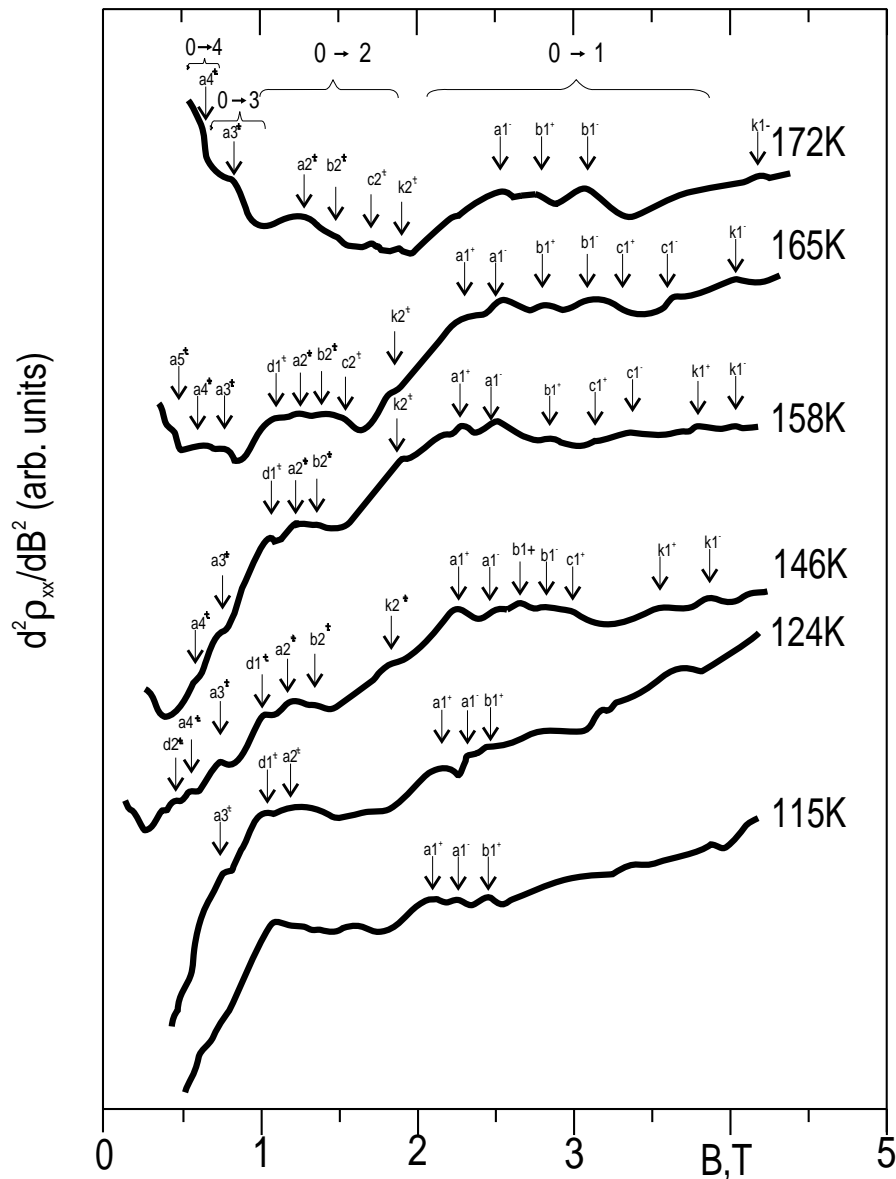| Positions of lines (cm^{-1})			
Sample I	Sample II	Sample III	Interpretation
118	118	118	TO HgTe cluster
121	122	123	TO HgTe-like lattice
142	143	143	TO CdTe-like lattice
—	165–182	163	TO ZnTe-like lattice
—	—	180	TO ZnTe cluster

Figure 2. Experimental records of $d^2\rho_{xx}(B)/dB^2$ obtained for sample IV at different temperatures (the temperatures are indicated to the right of the traces).

sample II: 7% of ZnTe; and sample III: 12% of ZnTe) are shown in figure 1. The comparison of the two curves for very small content of ZnTe (curve I) and with 7% of ZnTe (curve II) shows that the addition of ZnTe causes the appearance of salient in the range 160–180 cm^{-1}. This salient is split into two distinct lines at 163 cm^{-1} and 180 cm^{-1} on increasing the amount of ZnTe to 12% (curve III). Also, several strong lines in all of the curves are observed within the range 100–150 cm^{-1}. The positions of these lines, for each curve, are represented in table 2, and they can be explained as being caused by TO phonons of CdTe- and HgTe-like sublattices. By analogy with Raman spectra for MCT [22] and for

$Zn_xCd_{1-x}Te$ (ZCT) [18], the strong lines at 121–123 cm^{-1} can be interpreted as relating to TO modes of the HgTe-like sublattice. On the other hand, the lines at 142–143 cm^{-1} can be connected with TO modes of the CdTe-like sublattice. However, LO modes should also appear in these spectra. We believe that the weak intensity of the lines originating from LO modes is a consequence of the experimental conditions†. For example, under the analogous conditions described in [21], the intensity of the LO lines—which are part of the Raman shift spectra of CdTe—was much less than that of the TO lines.

Undoubtedly, the line at 163 cm^{-1} (curve III) arises from the TO phonons of the ZnTe-like sublattice. The line frequency of 180 cm^{-1} is almost the same as the frequency of the TO phonons in binary ZnTe.

At 118 cm^{-1} a sharp line has been observed in curves I and III (for curve II it is inconspicuous). This frequency corresponds to TO phonons in binary HgTe.

The interpretation of the lines in the Raman spectra is given in table 2. It is important to note that these spectra are in direct conformity with the three-mode behaviour of phonon spectra for ZMCT solid solutions. The presence of ZnTe and HgTe clusters is apparent too‡.

4. The magnetophonon resonance data

MPR was observed for three samples: IV–VI. The measurements were performed in pulsed magnetic fields. The second derivative of the transverse magnetoresistance, $d^2\rho_{xx}(B)/dB^2$, as a function of the magnetic field B was registered up to 6.5 T at different temperatures within the range 77–200 K. The most detailed investigations were performed for sample IV. The experimental records obtained for this specimen at different temperatures are shown in figure 2.

When the temperature was increased above 124 K, a group of strong peaks (a wide maximum) appeared in the range from 2.0 to 3.8 T; the corresponding harmonics were at 1.0–1.9 T and 0.6–0.9 T. The peak a1$^+$ is the strongest and the most distinguishable for the range 124 K $\leqslant T \leqslant$ 158 K, whereas peak a1$^-$ is the most distinguishable for $T >$ 158 K.

These peaks correspond to the harmonics a2, a3 and a4, because a2, a3 and a4 are observed in fields which are approximately equal to $(1/2)B_0$, $(1/3)B_0$ and $(1/4)B_0$, respectively (B_0 is the resonance magnetic field for peak a1$^+$).

In a similar manner, another three series of peaks can be determined—series b, c and k. Therefore, the structure of the wide maxima—which are clearly visible in the experimental curves in figure 2 at temperatures above 124 K—correspond to four series of peaks. These series are connected with four kinds of phonon.

A similar investigation, represented by the experimental records in figures 3 and 4, was conducted on specimens V and VI, respectively, for which $x + y$ is significantly larger and, correspondingly, the effective mass of the electrons is also greater. Consequently, the whole system of resonances is shifted to higher magnetic fields and, as can be seen for specimens V and VI, the same series of peaks, series a, b, c and k, are observed.

From these general considerations, it follows that the series a arises from the absorption of LO phonons of the HgTe-like sublattice, since these phonons have the lowest energy and they are present in the greatest numbers in the lattice of ZMCT. However, the energy of the LO phonons which can participate in electron–phonon interactions in this lattice has to be determined for the correct interpretation of the MPR data.

† The selection rules can be applied only for Raman spectra obtained using polarized light.
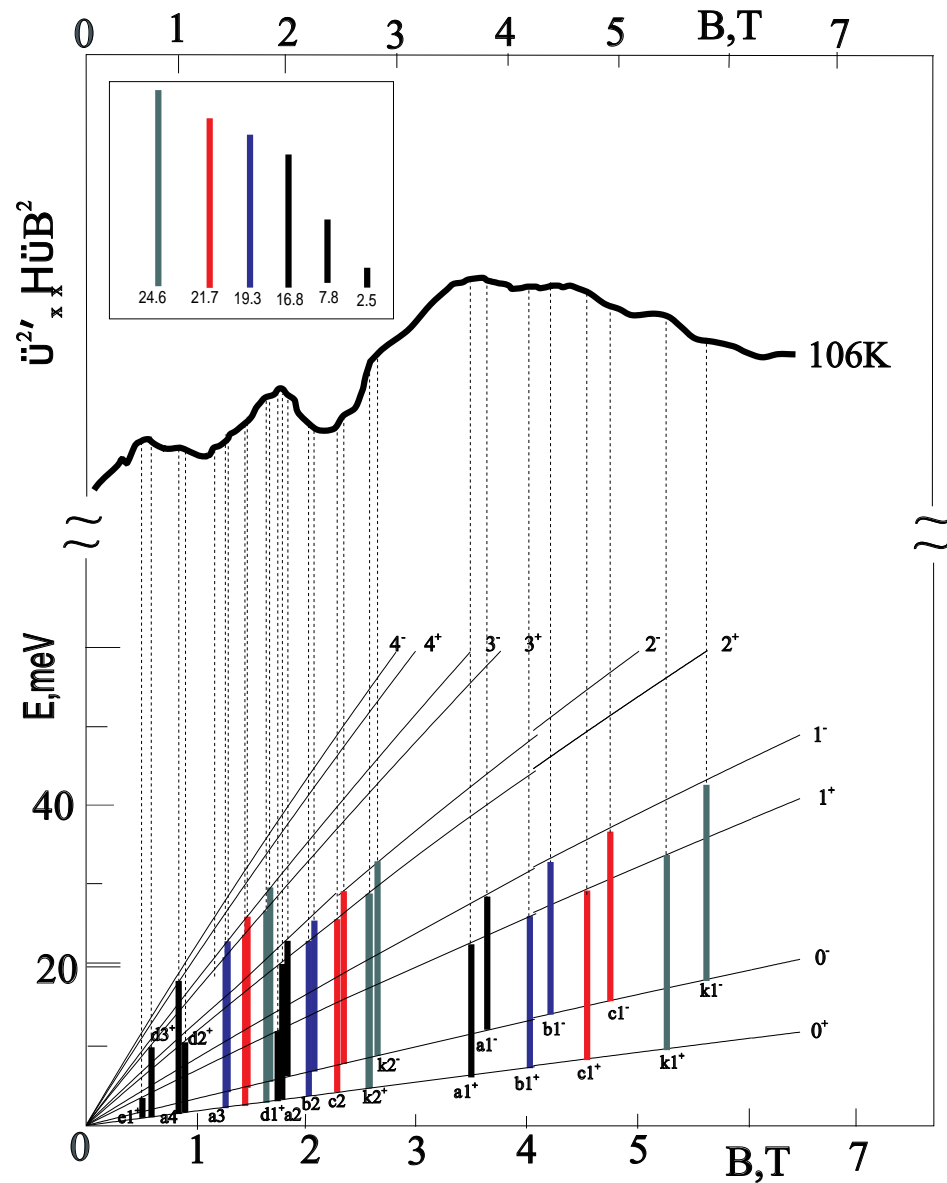‡ The existence of ZnTe clusters is confirmed by reflection–absorption spectra for the same ZMCT samples [23].

Figure 3. Experimental records of $d^2\rho_{xx}(B)/dB^2$ obtained for sample V at the temperature 106 K. The electron transitions between the Landau levels corresponding to observed MPRs are shown below. The inset shows the energy transitions appropriate to phonon energies or the differences of phonon energies (the values are given in meV).

5. The calculation of LO-phonon frequencies

Since it is impossible to determine LO-phonon frequencies for HgTe-like, CdTe-like and ZnTe-like sublattices from Raman spectra, the property of dielectric functions that the LO-phonon frequency can be extracted as a root from the equation $\mathrm{Re}\,\tilde{\varepsilon} = 0$ should be invoked [24]. This method was implemented in [25] for a multimode case. As follows from [25],
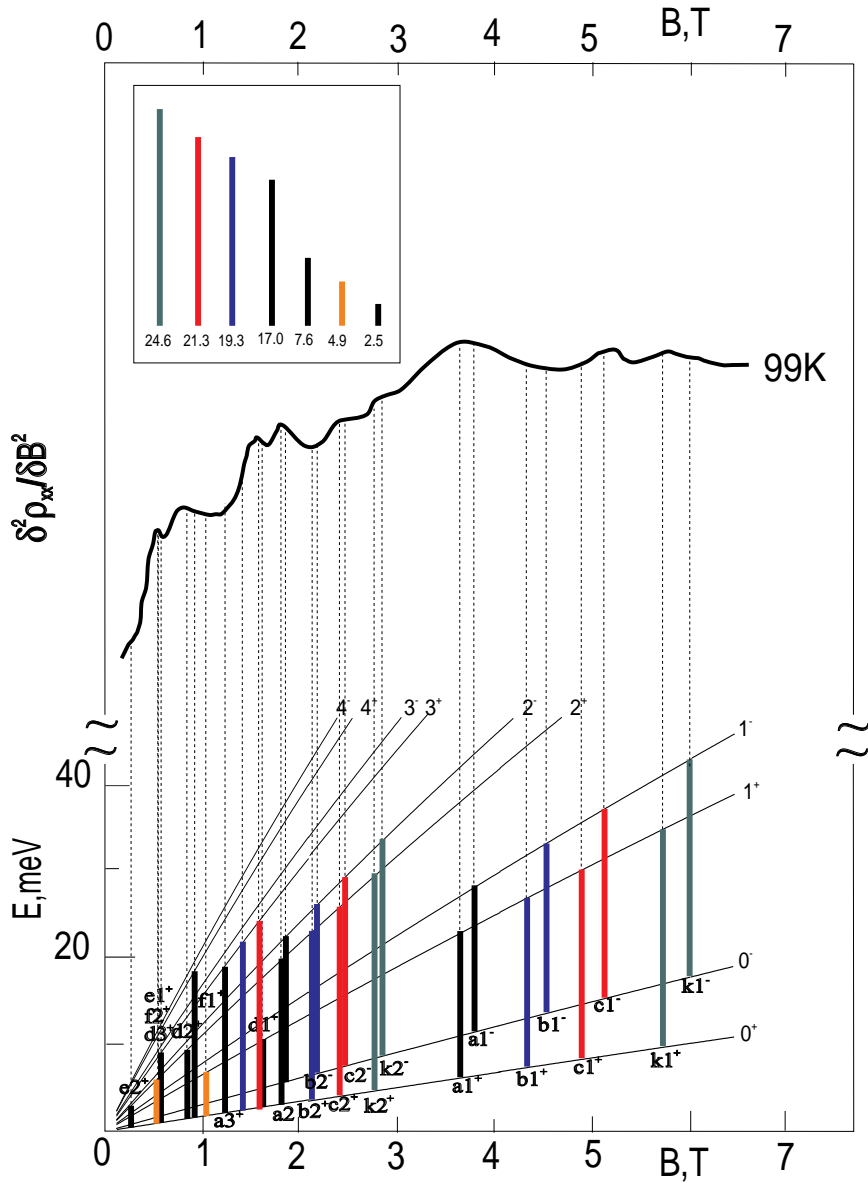
Figure 4. Experimental records of $d^2\rho_{xx}(B)/dB^2$ obtained for sample VI at the temperature 99 K. The electron transitions between the Landau levels corresponding to observed MPRs are shown below. The inset shows the energy transitions appropriate to phonon energies or the differences of phonon energies (the values are given in meV).

the dielectric function is constructed as the sum of three oscillators corresponding to the three sublattices of solid-solution crystals. Using the Lorentzian for each oscillator, we obtain

$$\varepsilon_\infty + \frac{S_1(\omega_{TO1}^2 - \omega^2)}{(\omega_{TO1}^2 - \omega^2)^2 + \omega^2\gamma_1^2} + \frac{S_2(\omega_{TO2}^2 - \omega^2)}{(\omega_{TO2}^2 - \omega^2)^2 + \omega^2\gamma_2^2} + \frac{S_3(\omega_{TO3}^2 - \omega^2)}{(\omega_{TO3}^2 - \omega^2)^2 + \omega^2\gamma_3^2} = 0 \qquad (1)$$
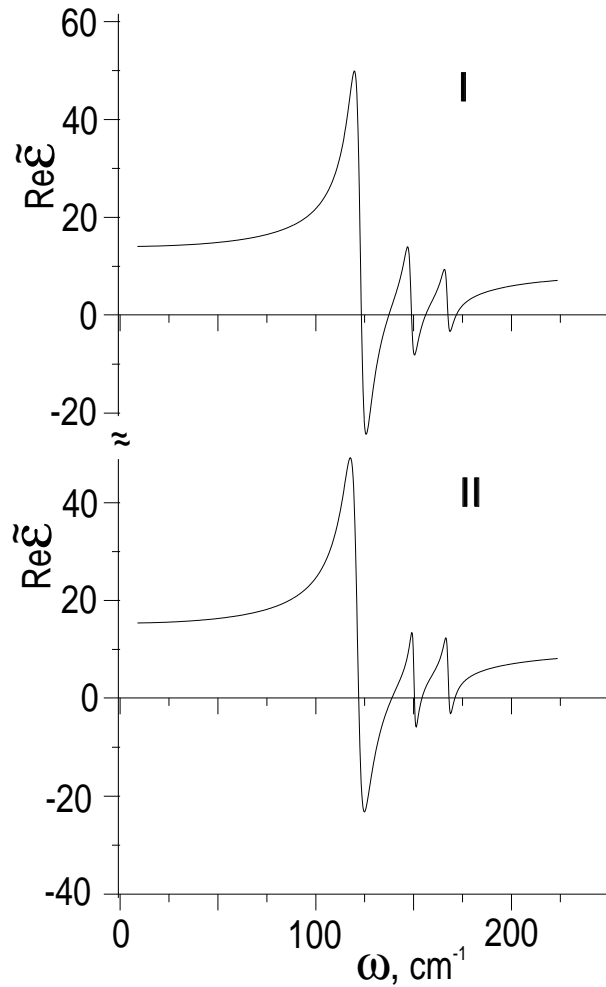
Figure 5. The real part of the dielectric function $\mathrm{Re}\,\tilde{\varepsilon}(\omega)$ for two compositions: curve I: for composition II; and curve II: for composition IV. The oscillator parameters are as follows. Composition II: HgTe-like lattice: $\omega_{\mathrm{TO1}} = 122\ \mathrm{cm}^{-1}$, $S_1 = 56\,020\ \mathrm{cm}^{-2}$, $\gamma_1 = 6.6\ \mathrm{cm}^{-1}$; CdTe-like lattice: $\omega_{\mathrm{TO2}} = 143\ \mathrm{cm}^{-1}$, $S_2 = 12\,960\ \mathrm{cm}^{-2}$, $\gamma_2 = 5.5\ \mathrm{cm}^{-1}$; ZnTe-like lattice: $\omega_{\mathrm{TO3}} = 165\ \mathrm{cm}^{-1}$, $S_3 = 6720\ \mathrm{cm}^{-2}$, $\gamma_3 = 5.5\ \mathrm{cm}^{-1}$; $\varepsilon_\infty = 10.0$. The solutions of equation (1) are: $\omega_1 = 127.8\ \mathrm{cm}^{-1}$, $\omega_2 = 136.4\ \mathrm{cm}^{-1}$, $\omega_3 = 148.7\ \mathrm{cm}^{-1}$, $\omega_4 = 156.8\ \mathrm{cm}^{-1}$, $\omega_5 = 167.9\ \mathrm{cm}^{-1}$, $\omega_6 = 172.4\ \mathrm{cm}^{-1}$. Composition IV: HgTe-like lattice: $\omega_{\mathrm{TO1}} = 121\ \mathrm{cm}^{-1}$, $S_1 = 63\,800\ \mathrm{cm}^{-2}$, $\gamma_1 = 6.6\ \mathrm{cm}^{-1}$; CdTe-like lattice: $\omega_{\mathrm{TO2}} = 144\ \mathrm{cm}^{-1}$, $S_2 = 7787\ \mathrm{cm}^{-2}$, $\gamma_2 = 5.5\ \mathrm{cm}^{-1}$; ZnTe-like lattice: $\omega_{\mathrm{TO3}} = 165\ \mathrm{cm}^{-1}$, $S_3 = 7680\ \mathrm{cm}^{-2}$, $\gamma_3 = 5.5\ \mathrm{cm}^{-1}$; $\varepsilon_\infty = 10.5$. The solutions of equation (1) are: $\omega_1 = 121.6\ \mathrm{cm}^{-1}$, $\omega_2 = 137.1\ \mathrm{cm}^{-1}$, $\omega_3 = 150.2\ \mathrm{cm}^{-1}$, $\omega_4 = 155.8\ \mathrm{cm}^{-1}$, $\omega_5 = 167.2\ \mathrm{cm}^{-1}$, $\omega_6 = 171.4\ \mathrm{cm}^{-1}$.

where the parameters S_i and γ_i represent the oscillator strength and damping factor of a particular mode, respectively, and ε_∞ stands for the high-frequency dielectric constant of a layer.

The oscillator strength S_i of the modes was chosen taking into account the composition of the solid solutions ZMCT: $S_1 = S_{\mathrm{HgTe}}(1 - x - y)$, $S_2 = S_{\mathrm{CdTe}}y$, $S_3 = S_{\mathrm{ZnTe}}x$. The values of the oscillator strength of the binary components from [12, 26, 27] have been used. The

value of ε_∞ can be determined from the composition dependence for MCT as specified in [12], by using $x + y$ (the total content of telluride, cadmium and zinc in ZMCT) instead of x, the latter standing for the cadmium telluride content. This is possible because the high-frequency dielectric constants of ZnTe and CdTe are nearly equal. Figure 5 shows the dielectric function $\text{Re}\,\varepsilon(\omega)$ for composition II (curve I). The parameters of the oscillators used in the calculations are given in the figure caption. The roots of equation (1) are also provided in the figure caption, where the even numbers stand for the frequencies of longitudinal phonons for corresponding sublattices (the first and the second roots were used for the corresponding HgTe-like sublattice, whereas the third and the fourth ones were used for the corresponding CdTe-like sublattice, and the fifth and the sixth ones were used for the corresponding ZnTe-like sublattice).

Table 3. Values of LO(Γ)-phonon frequencies and energies for compositions II and VI, and III and VI.

		HgTe-like mode	CdTe-like mode	ZnTe-like mode	ZnTe cluster
Composition II	ω_{LO} (cm^{-1}):	136	157.0	172.0	198.0
Composition II	$\hbar\omega_{LO}$ (meV):	16.8	19.5	21.4	24.6
Composition IV	ω_{LO} (cm^{-1}):	137	156.0	171.5	198.0
Composition IV	$\hbar\omega_{LO}$ (meV):	17.0	19.3	21.3	24.6
Composition III	ω_{LO} (cm^{-1}):	135.5	156.5	174.0	198.0
Composition III	$\hbar\omega_{LO}$ (meV):	16.7	19.4	21.7	24.6
Composition V	ω_{LO} (cm^{-1}):	136.0	156.0	174.0	198.0
Composition V	$\hbar\omega_{LO}$ (meV):	16.8	19.3	21.7	24.6
Composition VI	ω_{LO} (cm^{-1}):	136.0	156.0	175.0	198.0
Composition VI	$\hbar\omega_{LO}$ (meV):	16.8	19.3	21.9	24.6

Curve 2 in figure 5 shows the dependency $\text{Re}\,\tilde{\varepsilon}(\omega)$ for the parameters of the oscillators which were rectified for composition IV, characterized by a slightly lower cadmium content as compared to composition II. The oscillator strengths and high-frequency dielectric constant for composition IV were similarly determined, i.e. by substituting in the corresponding values of x and y. The magnitudes of the frequencies for the three modes were changed according to the typical composition dependencies of the optical phonon frequencies (see [12] and [18]). From this it follows that the decrease of the molar content of one binary compound in a solid solution leads to the frequencies of longitudinal and transverse optical phonons of given sublattices becoming similar, and vice versa. Therefore, we can predict that the decrease of the CdTe content (with the respective increase of the HgTe content with a constant ZnTe content) should slightly decrease ω_{TO} for the HgTe-like sublattice and increase ω_{TO} for the CdTe-like sublattice, whereas the frequency of the optical phonons in the ZnTe sublattice will be left unchanged or be insignificantly changed. This change of ω_{TO} in going from composition II to composition IV may be evaluated on the basis of the aforementioned compositional dependencies of phonon frequencies in MCT [12]. From this it follows that with a 1% decrease of the cadmium content, the frequency of TO phonons in the HgTe-like sublattice decreases at approximately 0.1 cm^{-1}. Simultaneously, the frequency of TO phonons in the CdTe-like sublattice increases at the same rate. The frequencies of ω_{TO} for composition IV for the

HgTe-like, CdTe-like and ZnTe-like sublattices were assumed to be equal to 121 cm^{-1}, 144 cm^{-1} and 165 cm^{-1} respectively. The parameters of oscillators using which Re $\tilde{\varepsilon}(\omega)$ was calculated for composition IV, as well as the solutions for equation (1), are provided in the caption of figure 5. This calculation of the frequencies of the longitudinal optical phonons and their energy for composition IV (measurements of MPR for this composition were also carried out) are shown in table 3. The values of ω_{LO} and $\hbar\omega_{LO}$ for composition II are given here for comparison with the values for composition IV.

Analogous studies were performed for composition V (which is close to composition III) with the aim of determining the phonon frequencies. The magnitudes of the LO-phonon frequencies and energies for this pair of compositions are presented in table 3 also.

The phonon frequencies for composition VI can be predicted on the basis of the composition tendencies obtained. In this case we have (in comparison to those for composition V) an increase of the zinc telluride content (by about 5%), a decrease of the cadmium telluride content (by about 2%) and a mercury telluride content of about of 3%. That means that the LO- and TO-phonon frequencies for the ZnTe-like sublattice diverge and converge, respectively, for the CdTe-like as well as HgTe-like sublattices. The increase (in comparison to that for composition V) of the LO-phonon frequency for the ZnTe-like sublattice can be estimate as 1 cm^{-1}, and the decrease of the same frequency for the HgTe-like sublattice is not more than 0.5 cm^{-1} (the changes of the phonon frequencies for CdTe are negligible). The frequencies and energies of the LO phonons for composition VI are given in table 3 also. The value of the frequency of the LO phonons for ZnTe clusters obtained from reflection–absorption spectra [23] is used here.

6. Interpretation of magnetophonon resonances

It follows from the considerations above that peaks a1$^+$ and a1$^-$—the strongest and the most distinguishable for $T > 124$ K in the experimental curves in figures 2–4, and characterized by harmonics at corresponding magnetic fields—are caused by the electron transitions 0$^+$– 1$^+$ and 0$^-$–1$^-$ accompanied by the absorption of LO phonons of the HgTe-like sublattice. Our further interpretation of the MPR spectra is based on this assumption, which enables us to estimate to a first approximation the parameters of the band structure using the energy value of the LO phonons of the HgTe-like sublattice from table 3 and the experimental positions in the magnetic field of the peaks a1$^+$ and a1$^-$.

The band-structure parameters have been calculated according to Aggrawal's version [28] of the Pidgeon–Brown model [29]. This method is based on the three-level Kane model [30], which is a good approximation for narrow-gap semiconductors, whereas the five-level model is more useful for wide-gap ones [31, 32]. Luttinger's procedure [33] for the calculation of valence-band Landau level energies is implemented here. In the Pidgeon–Brown model, γ_1, γ_2, γ_3 and K are the valence-band parameters due to the higher-band contributions:

$$\gamma_1 = \gamma_1^{L} - \frac{E_p}{3E_g}$$

$$\gamma_2 = \gamma_2^{L} - \frac{E_p}{6E_g}$$

$$\gamma_3 = \gamma_3^{L} - \frac{E_p}{6E_g}$$

$$K = K^{L} - \frac{E_p}{6E_g}$$

where γ_1^L, γ_2^L, γ_3^L and K^L are the valence-band parameters defined by Luttinger [33] and E_g is the energy gap; E_p is the energy equivalent of the momentum matrix element connecting the conduction and valence band.

Experience has shown that the choice of the values of γ_1^L, γ_2^L, γ_3^L and K^L is crucial to the determination of the band-structure parameters for MCT [34–37] using the relations between them given below (as equations (2) and (3)). We have

$$\gamma_1^L = \frac{E_p}{3E_g} + 2.5$$
$$\gamma_2^L = \gamma_3^L = \frac{E_p}{6E_g}. \tag{2}$$

It has been assumed that $E_p = 18.0$ eV and $\Delta = 1.0$ eV [34], and that they do not depend on the temperature and composition. According to [38], the next parameter, K^L, should be represented as follows:

$$K^L = \gamma_3^L - \frac{1}{3}\gamma_1^L + \frac{2}{3}\gamma_2^L - \frac{2}{3} - \frac{5}{4}\delta_{\text{exch}} \tag{3}$$

where δ_{exch} stands for the correction for the nonlocality of the potential and is equal to 0.4 for MCT [39]. As for the last parameter, F, representing the interaction of the conduction band with the upper bands, we have used the value $F = -0.5$ determined by Weiler *et al* [34]. We have assumed that this parameter is also not dependent on the temperature and composition.

Table 4. The band-structure parameter values for samples IV–VI.

Parameters	Sample IV 146 K	Sample IV 165 K	Sample V 106 K	Sample VI 99 K
E_g (meV)	192	205	320	350
E_p (meV)	18 000	18 000	18 000	18 000
γ_1^L	33.75	31.7	21.25	19.64
$\gamma_2^L = \gamma_3^L$	15.62	14.6	9.38	8.57
K^L	13.62	12.6	7.38	6.57
F	−0.5	−0.5	−0.5	−0.5
Δ (meV)	1000	1000	1000	1000

In order to calculate the theoretical positions of the MPR peaks, we applied the best-fit procedure to the experimental positions of peaks a1$^+$ and a1$^-$, thus obtaining the value of the energy $E_g = 190$ meV at the temperature $T = 146$ K. The next step in the calculation procedure is that of fitting the theoretical positions of all of the observed peaks of the a series to the experimental ones at a given temperature. The best fits are shown in figure 6 for $T = 146$ K and figure 7 for $T = 165$ K, where the electron transitions corresponding to resonance peaks of series a are shown by solid arrows. We can see a good agreement between the experimental and theoretical positions of resonances (the average disparity for eight peaks of series a$^+$ and a$^-$ on the curve at 146 K is equal to approximately 1.5%). The thus-obtained band parameters for $T = 146$ K and 165 K are shown in table 4. Now, it is possible to interpret the other series of peaks, namely series b, c and k. Since the positions of peaks b1$^+$, c1$^+$ and k1$^+$ are characterized by an increase in the magnetic field, these peaks may be expected to be caused by electron transitions 0$^+$–1$^+$ with the
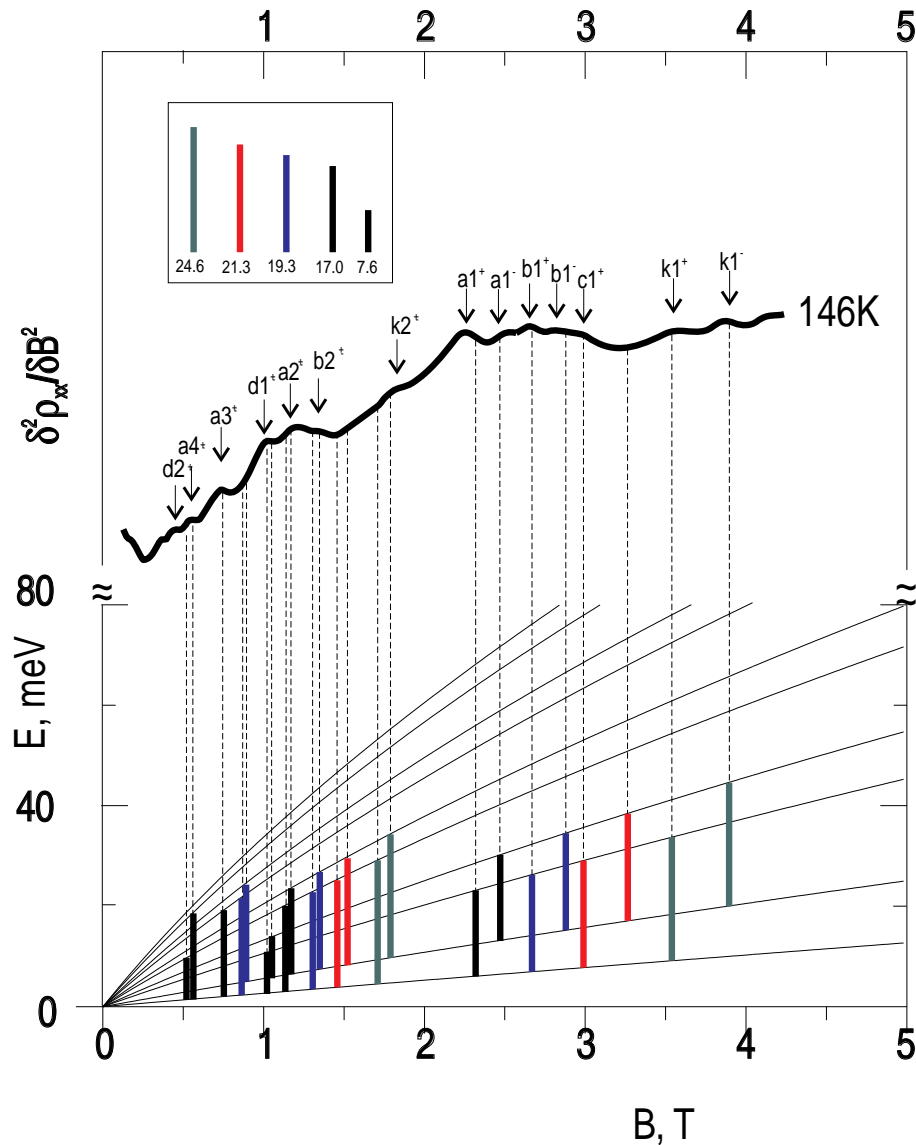
Figure 6. Experimental records of $d^2\rho_{xx}(B)/dB^2$ obtained for sample IV at the temperature 146 K. The electron transitions between the Landau levels corresponding to observed MPRs are shown below. The inset shows the energy transitions appropriate to phonon energies or the difference of phonon energies (the values are given in meV).

accompanying absorption of LO phonons of, consequently, increasing frequencies. This sequence of increasing frequencies corresponds to the LO phonons in CdTe-like and ZnTe-like sublattices and ZnTe clusters. The theoretical positions of the MPRs for all of the series were calculated using the aforementioned band-structure parameters (see table 4 for $T = 146$ K and 165 K) and phonon energies (table 3), whereas the general interpretation of the observed experimental peaks (figure 2) is given in table 5. The overall representation of the electron transitions which can be used to interpret the observed MPR peaks may be found
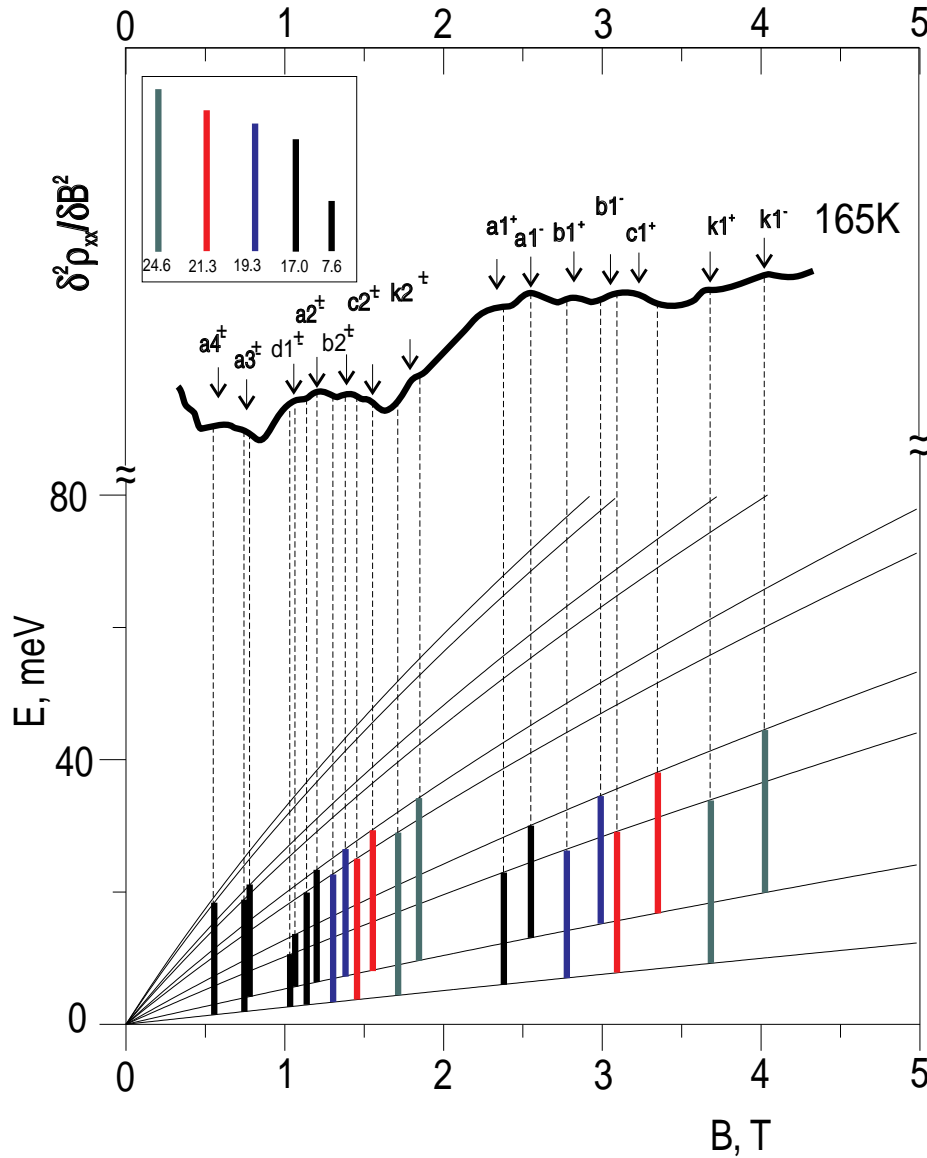
Figure 7. Experimental records of $d^2\rho_{xx}(B)/dB^2$ obtained for sample IV at the temperature 165 K. The electron transitions between the Landau levels corresponding to observed MPRs are shown below. The inset shows the energy transitions appropriate to phonon energies or the difference of phonon energies (the values are given in meV).

in figures 6 and 7. This shows that the suggested interpretation of MPR peaks based on the application of four kinds of LO phonon is in good agreement with the experimentally observed structure of the resonance curves. Simultaneously, the quantitative agreement between the calculated positions of the corresponding electron transitions in the magnetic field and the observed peaks of the four series is within about 1.5% (the measurement accuracy of the resonance fields is ∼3%). The comparison of the two curves (the first one at 146 K and the second at 165 K) reveals that the increase in the temperature is accompanied

Table 5. General interpretation of MPR peaks (sample IV).

Peak symbol	Interpretation	Resonance fields (T)			
		$T = 146$ K		$T = 165$ K	
		Experiment ($\pm 3\%$)	Theory	Experiment ($\pm 3\%$)	Theory
a1$^+$	$0^+ \to 1^+ + \text{LO}(\Gamma)$-phonon HgTe-like lattice	2.26	2.30	2.35	2.42
a1$^-$	$0^- \to 1^- + \text{LO}(\Gamma)$-phonon HgTe-like lattice	2.45	2.44	2.51	2.56
a2	$0^+ \to 2^+ + \text{LO}(\Gamma)$-phonon HgTe-like lattice	1.16	1.14	1.20	1.20
	$0^- \to 2^- + \text{LO}(\Gamma)$-phonon HgTe-like lattice	1.16		1.22	
a3	$0^+ \to 3^+ + \text{LO}(\Gamma)$-phonon HgTe-like lattice	0.76	0.74	0.75	0.78
	$0^- \to 3^- + \text{LO}(\Gamma)$-phonon HgTe-like lattice		0.76		0.80
a4	$0^+ \to 4^+ + \text{LO}(\Gamma)$-phonon HgTe-like lattice	0.54	0.55	0.59	0.58
	$0^- \to 4^- + \text{LO}(\Gamma)$-phonon HgTe-like lattice		0.56		0.59
b1$^+$	$0^+ \to 1^+ + \text{LO}(\Gamma)$-phonon CdTe-like lattice	2.64	2.68	2.80	2.82
b1$^-$	$0^- \to 1^- + \text{LO}(\Gamma)$-phonon CdTe-like lattice	2.87	2.90	3.05	3.04
b2	$0^+ \to 2^+ + \text{LO}(\Gamma)$-phonon CdTe-like lattice	1.33	1.30	1.39	1.38
	$0^- \to 2^- + \text{LO}(\Gamma)$-phonon CdTe-like lattice		1.36		1.44
c1$^+$	$0^+ \to 1^+ + \text{LO}(\Gamma)$-phonon ZnTe-like lattice	2.99	3.00	3.22	3.16
c1$^-$	$0^- \to 1^- + \text{LO}(\Gamma)$-phonon ZnTe-like lattice	—	3.26	—	3.42
c2	$0^+ \to 2^+ + \text{LO}(\Gamma)$-phonon ZnTe-like lattice	—	1.46	1.55	1.54
	$0^- \to 2^- + \text{LO}(\Gamma)$-phonon ZnTe-like lattice		1.52		1.60
k1$^+$	$0^+ \to 1^+ + \text{LO}(\Gamma)$-phonon ZnTe cluster	3.62	3.60	3.69	3.78
k1$^-$	$0^- \to 1^- + \text{LO}(\Gamma)$-phonon ZnTe cluster	3.90	3.96	4.02	4.14
k2$^+$	$0^+ \to 2^+ + \text{LO}(\Gamma)$-phonon ZnTe cluster	1.82	1.74	1.79	1.82
k2$^-$	$0^- \to 2^- + \text{LO}(\Gamma)$-phonon ZnTe cluster	1.82	1.82	1.79	1.90
d1$^+$	MPR on the difference of phonon frequencies	1.0	1.04	1.04	1.08

with an increase of the amplitudes of the peaks a1$^-$ and a2$^-$. This observation is also made for the peaks of another series, in this case caused by electron transitions between 0^- and N^- Landau levels. It is obvious that the increase of temperature causes the increase of the electron occupation of the 0^- Landau level and the increase in the amplitude of the aforementioned peaks. Nevertheless, the peaks of series d in the small magnetic fields are less visible at temperatures higher than 124 K (for sample IV).

The same method for calculation of the band-structure parameters and interpretation of the MPR peaks using the phonon energies given in table 3 is applied to samples V and VI. The values of the band-structure parameters determined for these samples from MPR data are represented in table 4. Figures 3 and 4 highlight the electron transitions corresponding to the resonance peaks. One can notice that peak a1 also dominates for the compositions V and VI. The resonances caused by the LO phonons of the CdTe-like and ZnTe-like sublattices and ZnTe clusters appear on its wing at high magnetic fields. On the other hand, the first harmonics (transitions 0–2) of the same resonances are visible on the slope of peak a1 at a weaker magnetic field, but those amplitudes are, obviously, smaller. This explains the significant broadening of this peak. Simultaneously, two peaks at 1.6–1.8 T and 0.5–0.7 T in the experimental curves mentioned above are too strong to be the first and the second harmonics of the resonance a1.
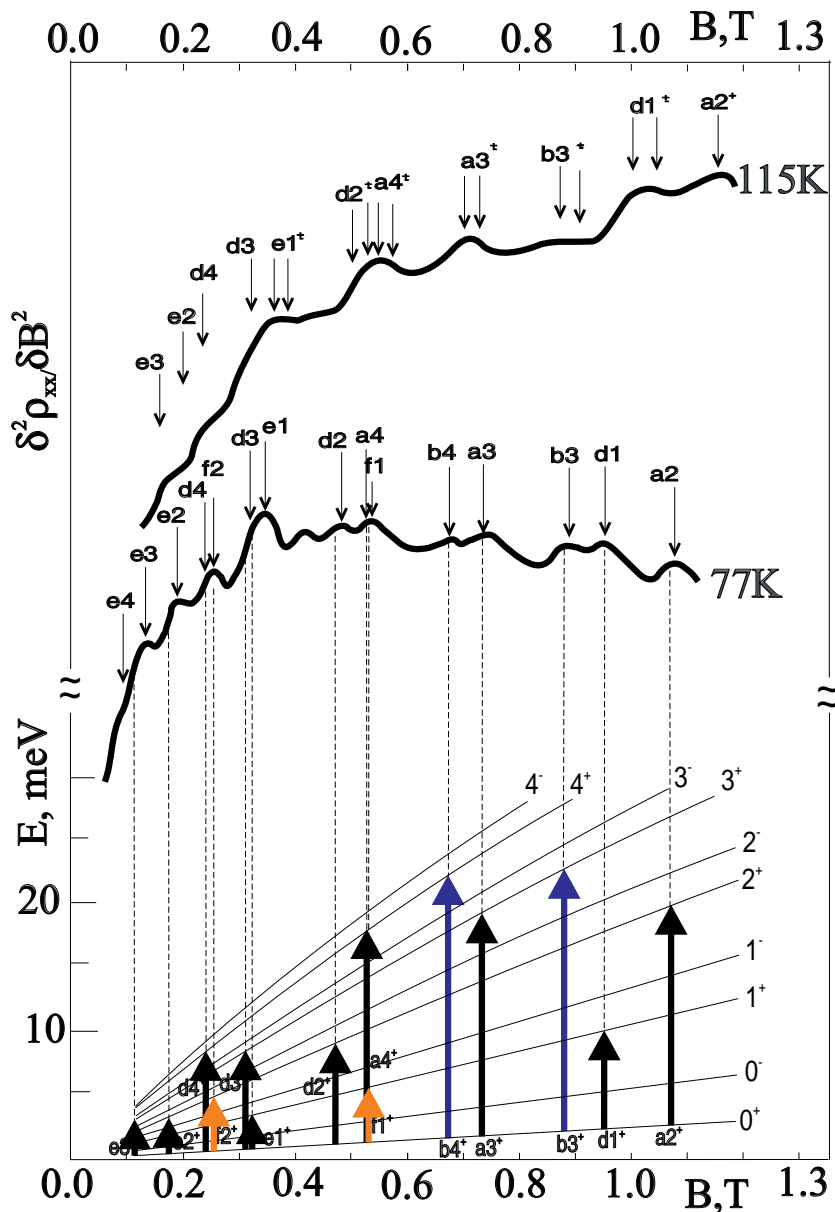
Figure 8. Experimental records of $d^2\rho_{xx}(B)/dB^2$ obtained for sample IV at the temperatures 77 K and 115 K on a smaller magnetic field scale than that used in figures 6 and 7. The electron transitions between the Landau levels corresponding to observed MPRs are shown below.

7. Magnetophonon resonance on the difference of phonon frequencies (MPR DPF)

The complicated structure of the peaks in a weak magnetic field is of special interest, because it cannot be interpreted as higher harmonics of the four types of MPR described above. In our previous paper [11], the temperature behaviour of the amplitudes and positions of the peaks in the magnetic fields belonging to the d series as well as the e series were analysed

in detail (for the case of composition IV). That analysis confirmed the two-phonon nature of these resonances: they are MPRs with the simultaneous absorption and emission of phonons belonging to two different sublattices of a solid solution. It has been shown [11] that the transition energy for the d series is equal to about 8 meV, which equals the energy difference of (i) the LO phonons in binary ZnTe and (ii) the LO phonons of the HgTe-like sublattice for composition IV. It was difficult to comprehend why LO phonons of binary ZnTe arise in the solid solution of ZMCT. The Raman scattering data presented in this paper show that these LO phonons in the ZnTe binary lattice could be generated by ZnTe clusters in the solid solutions. The calculated phonon frequencies enable us to interpret these d and e series of resonances correctly for composition IV as well as for compositions V and VI.

Figure 8 shows experimental records for sample IV on a smaller magnetic field scale than that in figure 2. It is obvious that the d series begins from 0.95 T for 77 K for the d1 peak and continues to $\frac{1}{2} \times 0.95$ T and $\frac{1}{3} \times 0.95$ T for the d2 and d3 peaks respectively. In addition to the series of peaks d, there is another series of peaks marked as e, which behave similarly to the d peaks with the increase of temperature within this range of magnetic field. A peak e1 appears at 0.33 T on the curve for 77 K which cannot be interpreted as a harmonic of the resonances described above. The MPR curve for 77 K in figure 8 shows that the peaks marked as e2 and e3 are observable for the fractions 1/2 and 1/3, respectively, of the magnetic field at which peak e1 appears. Therefore, two new series of peaks have been observed in this region of the magnetic field. The same series appear in the curve obtained at 115 K, but they shift towards higher magnetic fields there.

Table 6. Interpretation of the series d and series e peaks in the region of small magnetic fields (sample IV).

| | | Resonance fields in T | | | |
| | | $T = 77$ K | | $T = 155$ K | |
Peak symbol	Interpretation	Theory	Experiment ($\pm 3\%$)	Theory	Experiment ($\pm 3\%$)
d1$^+$	$0^+ - 1^+ + \hbar\omega_{LO}$(ZnTe cluster) $- \hbar\omega_{LO}$(HgTe-like)	0.95	0.95	0.99	1.0
d1$^-$	$0^- - 1^- + \hbar\omega_{LO}$(ZnTe cluster) $- \hbar\omega_{LO}$(HgTe-like)	0.99	0.95	1.03	1.0
d2$^+$	$0^+ - 2^+ + \hbar\omega_{LO}$(ZnTe cluster) $- \hbar\omega_{LO}$(HgTe-like)	0.47	0.48	0.49	0.55
d2$^-$	$0^- - 2^- + \hbar\omega_{LO}$(ZnTe cluster) $- \hbar\omega_{LO}$(HgTe-like)	0.48	0.48	0.50	0.55
d3$^+$	$0^+ - 3^+ + \hbar\omega_{LO}$(ZnTe cluster) $- \hbar\omega_{LO}$(HgTe-like)	0.31	0.33	0.32	0.32
d3$^-$	$0^- - 3^- + \hbar\omega_{LO}$(ZnTe cluster) $- \hbar\omega_{LO}$(HgTe-like)	0.32	0.33	0.33	0.32
d4$^\pm$	$0^\pm - 4^\pm + \hbar\omega_{LO}$(ZnTe cluster) $- \hbar\omega_{LO}$(HgTe-like)	0.23	0.25	0.24	0.25
e1$^+$	$0^+ - 1^+ + \hbar\omega_{LO}$(CdTe-like) $- \hbar\omega_{LO}$(HgTe-like)	0.32	0.33	0.33	0.36
e1$^-$	$0^- - 1^- + \hbar\omega_{LO}$(CdTe-like) $- \hbar\omega_{LO}$(HgTe-like)	0.33	0.33	0.34	0.36
e2$^\pm$	$0^\pm - 2^\pm + \hbar\omega_{LO}$(CdTe-like) $- \hbar\omega_{LO}$(HgTe-like)	0.16	0.17	0.17	0.23
e3$^\pm$	$0^\pm - 3^\pm + \hbar\omega_{LO}$(CdTe-like) $- \hbar\omega_{LO}$(HgTe-like)	0.11	0.12	0.12	0.18
f1$^\pm$	$0^\pm - 1^\pm + \hbar\omega_{LO}$(ZnTe-like) $- \hbar\omega_{LO}$(HgTe-like)	0.52	0.52†	0.54	0.55†
f2$^\pm$	$0^\pm - 2^\pm + \hbar\omega_{LO}$(ZnTe-like) $- \hbar\omega_{LO}$(HgTe-like)	0.26	0.25‡	0.27	0.25‡

† Coincides with a4.
‡ Coincides with d4.

The interpretation of these series is performed by using the values of the phonon energies (table 3) and the band-structure parameters based on values of E_g equal to 175 meV and 183 meV at $T = 77$ K and 115 K, respectively. The theoretical positions of the three kinds of MPR DPF (at $\hbar\omega_{LO}$(ZnTe cluster) $- \hbar\omega_{LO}$(HgTe-like), $\hbar\omega_{LO}$(CdTe-like) $- \hbar\omega_{LO}$(HgTe-
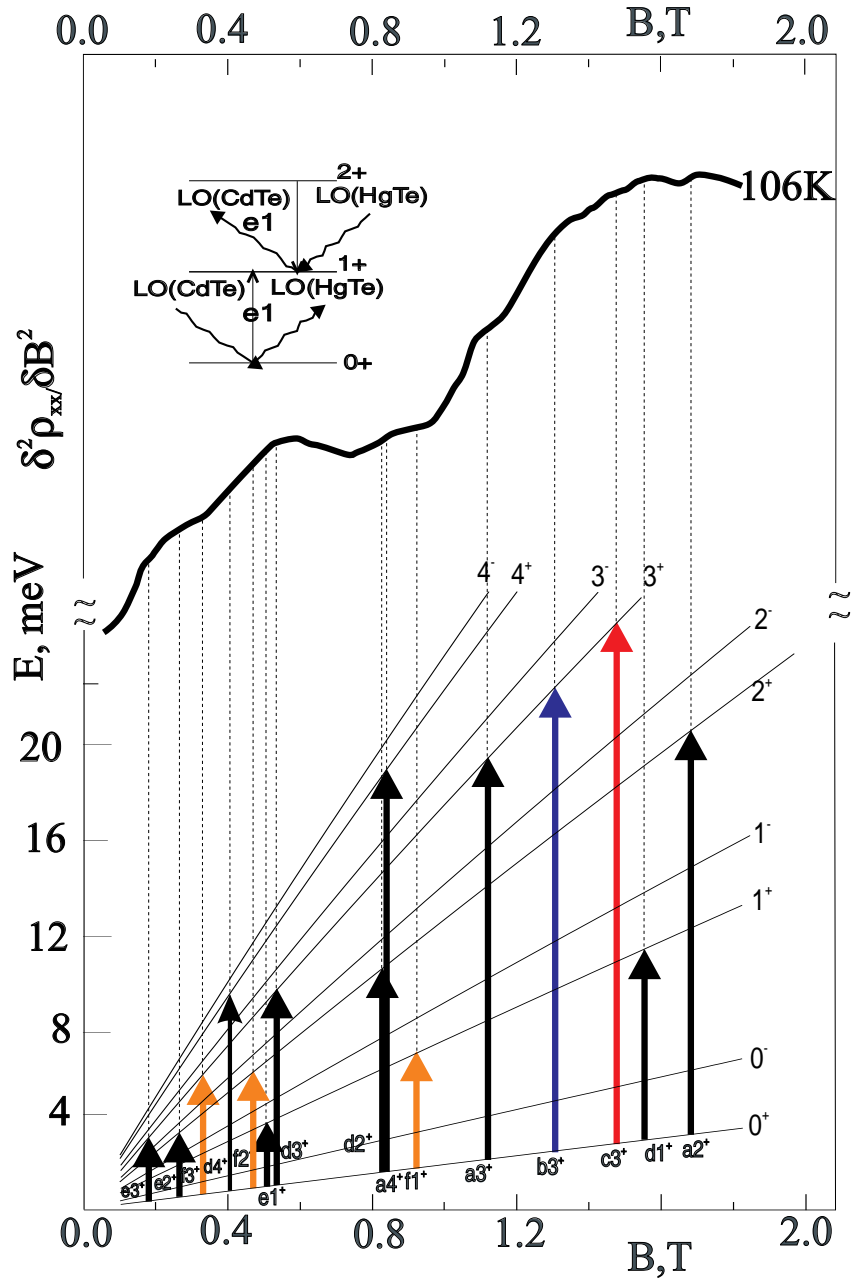
Figure 9. Experimental records of $\mathrm{d}^2\rho_{xx}(B)/\mathrm{d}B^2$ obtained for sample V at the temperature 106 K on a magnetic field scale smaller than that used in figure 3. The electron transitions between the Landau levels corresponding to observed MPRs are shown below.

like) and $\hbar\omega_{\mathrm{LO}}(\mathrm{ZnTe\text{-}like}) - \hbar\omega_{\mathrm{LO}}(\mathrm{HgTe\text{-}like}))$ are represented in table 6. The experimental positions of the peaks of series d, e and a (a2, a3, a4) are also specified in that table. The electron transitions corresponding to the resonance peaks are shown in figure 8.

The conclusion can be drawn that there is a good agreement between the experimental
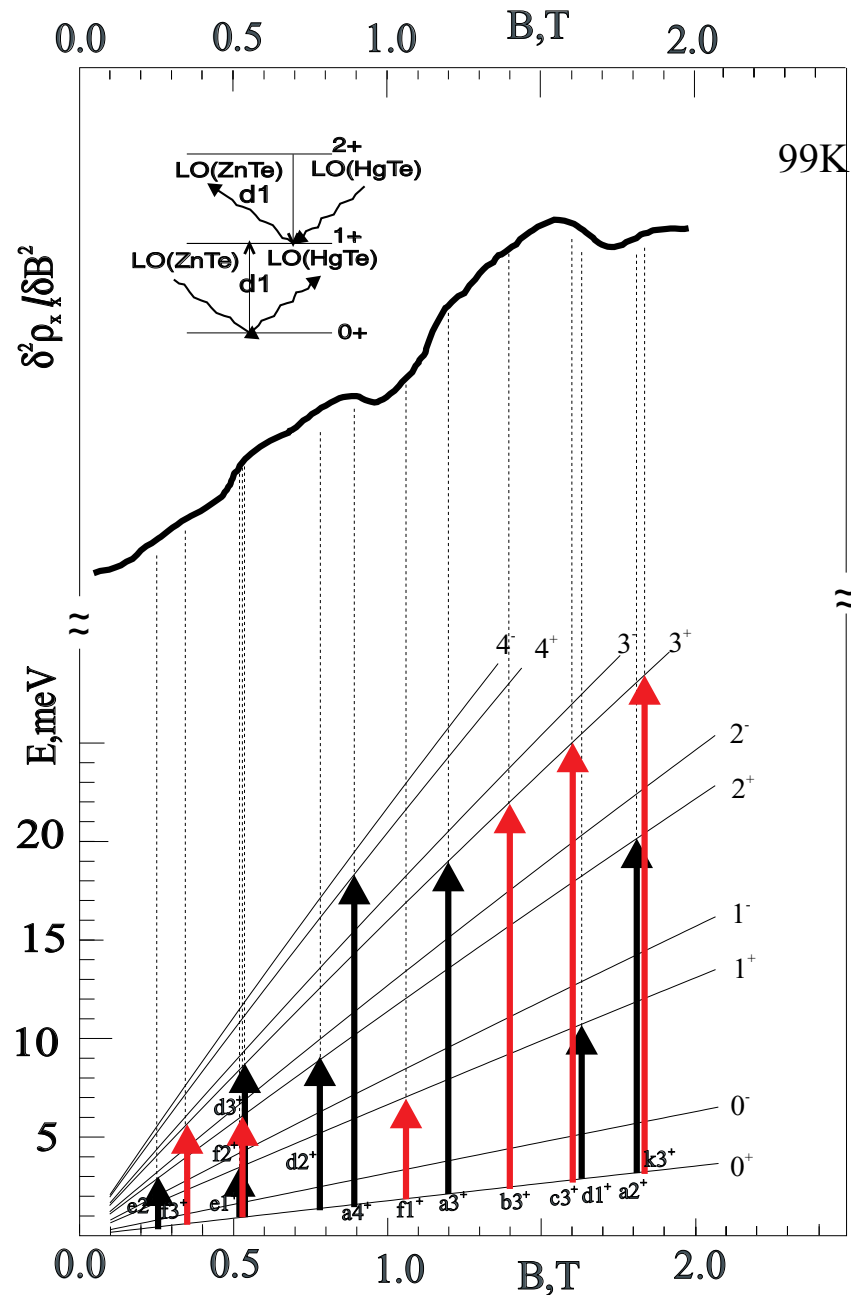
Figure 10. Experimental records of $d^2\rho_{xx}(B)/dB^2$ obtained for sample VI at the temperature 99 K on a magnetic field scale smaller than that used in figure 4. The electron transitions between the Landau levels corresponding to observed MPRs are shown below.

positions of the peaks of series d and e and the MPR DPF attributed to them. Thus, it can be stated that the resonance series d is caused by the transitions of electrons between the Landau levels with LO-phonon absorption in ZnTe clusters and emission of LO phonons in

the HgTe-like sublattice. The electron transitions accompanied by absorption of phonons in the CdTe-like sublattice and emission of phonons in the HgTe-like sublattice correspond to the e series. Moreover, an MPR DPF series with the absorption of LO phonons in the ZnTe-like sublattice and emission of LO phonons in the HgTe-like sublattice can be predicted theoretically for this region of magnetic fields. They are labelled as series f in figure 8 and table 6. Nevertheless, their existence cannot be unambiguously proved at this stage.

Similar studies were performed for specimen V (figure 9) and for specimen VI (figure 10). It is noteworthy that peak $d1^+$ is stronger than peak $a2^+$ for these specimens, which means that, in comparison to that for composition IV, the d series for the compositions V and VI are better manifested. However, again, in this case for the f series, it is impossible to give an unambiguous proof of existence.

8. Temperature dependencies of band parameters and the band-structure model with potential fluctuations

The previously evaluated band-structure parameters of samples IV–VI obtained on the basis of MPR peak positions correspond to the conduction electrons, which means that the former correspond to that part of the volume of the epitaxial layer investigated in which electrical conductivity was provided.

The x-ray microanalysis of the composition of the material showed that the sample of $Zn_xCd_yHg_{1-x-y}Te$ displays homogeneity down to a depth of about 4 μm (see the inset of figure 11). The Raman scattering data corroborate the assertion that the main part of the lattice has a three-mode phonon spectrum. The latter three-mode spectrum, in turn, affirms the stochastically homogeneous distribution of three cation atoms (Hg, Cd, Zn) surrounding the anion atom (Te). On the other hand, it can be deduced from the same Raman spectra that a certain part of the crystal volume is occupied by restricted regions, where the anion atom is surrounded by mostly Zn atoms (ZnTe clusters) or by Hg atoms (HgTe clusters).

It could be suggested that the electron transport occurs in a part of the crystal where a stochastically homogeneous distribution of cation atoms takes place. Undoubtedly, there are considerable fluctuations of the potential there, which to a great extent are 'washed out' by the sufficiently high electron concentration. So, it can be said that in this case the band structure is spatially uniform. It is actually this structure that the aforementioned band parameters determined from the MPR belong to.

The electrons go round the ZnTe clusters, where there are the high potential peaks, and hence these regions do not make any contribution to the conductivity. However, the long-range polarization fields induced by the long-wavelength longitudinal optical vibrations in those clusters influence the electron transport. They penetrate into those parts of the lattice where the electron transport takes place, and the electrons can be scattered by these fields, elastically or inelastically, the latter being noticeable for MPR.

In contrast, the regions where the HgTe clusters occur are characterized by deep potential valleys filled by the 'electron lakes'. They do not form a bundle of clusters; otherwise the electrons would transfer along these chains and the conductivity would be of an inactivated character. The macrofields induced here by LO phonons are screened due to the high local electron concentration and do not affect the electron transport within the lattice, i.e. do not take part in the MPR.

It can be safely assumed that a macrofield induced by the LO phonons of the ZnTe-like sublattice is more effectively screened by electrons in the 'homogeneous' part of the lattice for which those fields are internal, whereas a macrofield induced by the LO phonons of ZnTe
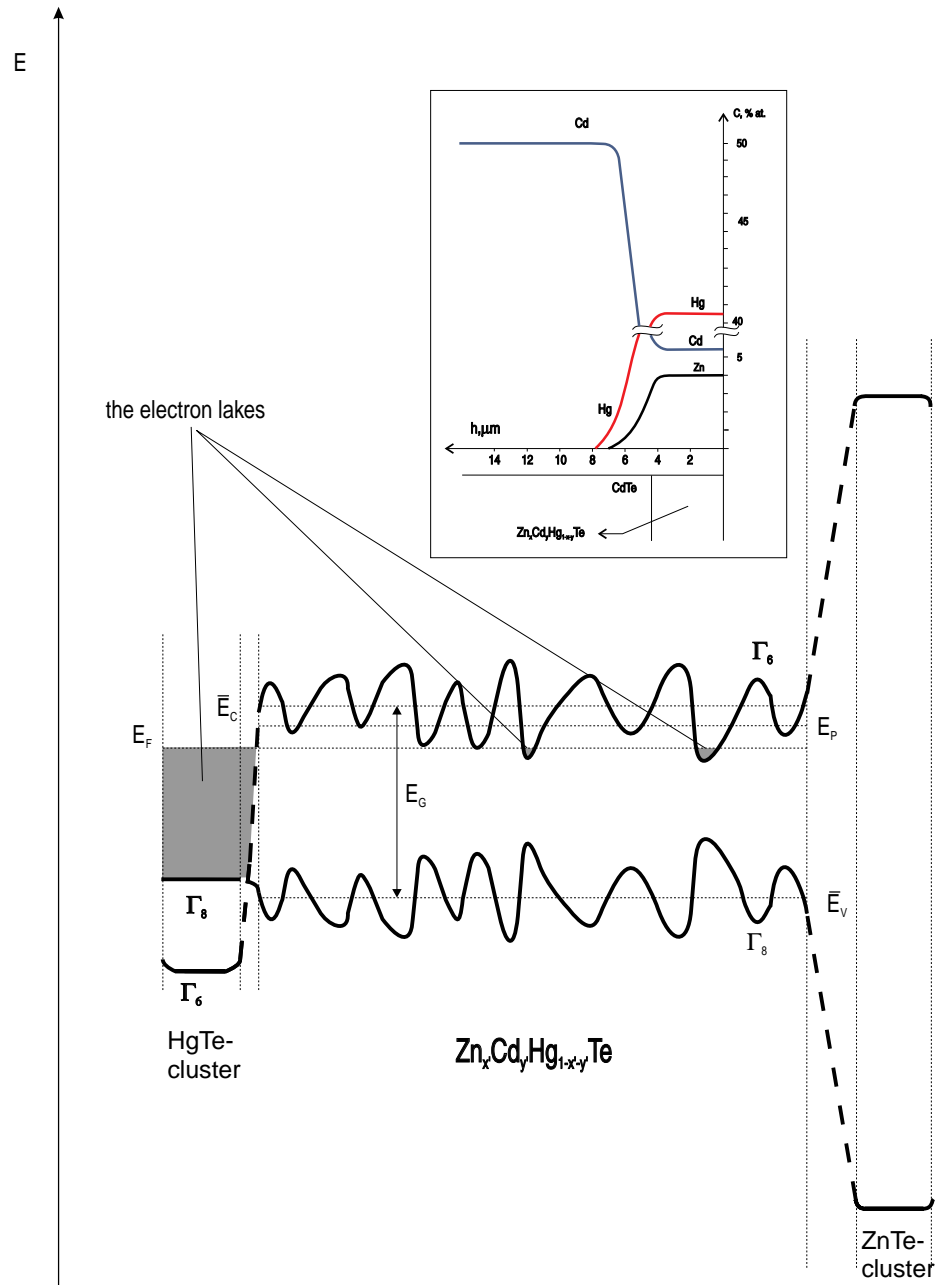
Figure 11. The band structure of ZMCT solid solutions with potential fluctuations. $\bar{E}_c$ and $\bar{E}_v$ are the average bottom of the conduction band and the average top of the valence band, respectively. E_p is the percolation level. The inset shows the depth profile of the epitaxial layer for sample IV.

clusters external to the electrons participating in the conductivity is screened less effectively. This can explain the fact that the amplitudes of the series k peaks are not smaller than those for series c. Moreover, series d is much more evident than series f.
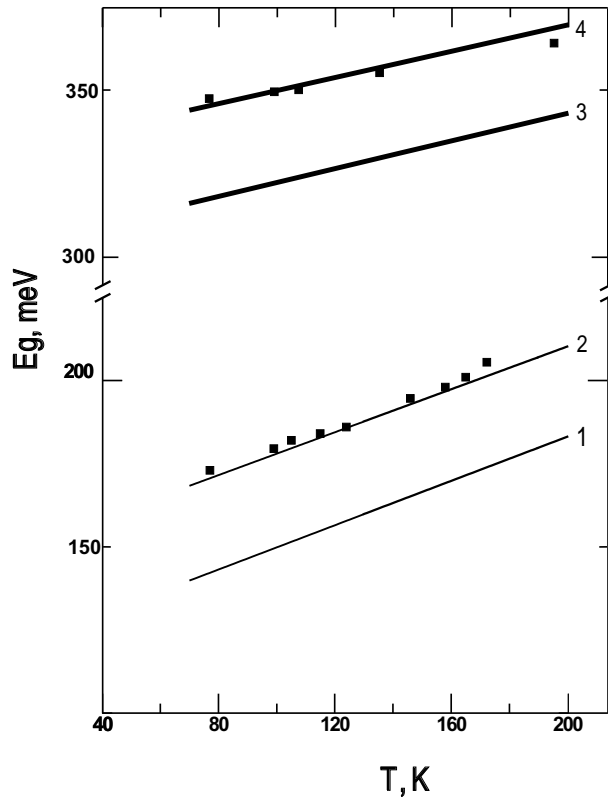
Figure 12. The temperature dependencies of the energy gap for compositions IV and VI. Full squares: the values of E_g obtained from the MPR. Curve 1 is calculated from the empirical dependence $E_g(x, y, T)$ for composition IV ($x = 0.08$, $y = 0.11$). Curve 2 is calculated from the empirical dependence $E_g(x, y, T)$ for the composition with $x' = 0.0775$, $y' = 0.13$. Curve 3 is calculated from the empirical dependence $E_g(x, y, T)$ for composition VI ($x = 0.17$, $y = 0.08$). Curve 4 is calculated from the empirical dependence $E_g(x, y, T)$ for the composition with $x'' = 0.1675$, $y'' = 0.1$.

Thus, the model proposed here and represented in figure 11 is in good agreement with MPR data as well with Raman spectroscopy data. The temperature dependence of the energy gap can be very well adjusted to the overall representation, too. The temperature shift of the MPR peaks provides us with the possibility to establish the temperature dependence of the energy gap E_g for the chosen temperature region.

The band-parameter calculation procedure using the MPR peak positions described above has been applied to all of the resonance curves obtained for samples IV–VI. The values of E_g determined from the MPR for samples IV and VI are represented by black squares in figure 12.

Of considerable interest is the comparison of the dependence of $E_g(T)$ obtained with those calculated by means of empirical formulae for the energy gap dependencies on the component concentration and temperature. The procedure for calculating $E_g(x, y, T)$ proposed in [3] has been implemented for the quaternary solid solutions of $Zn_xCd_yHg_{1-x-y}Te$ with common anion atoms. Three empirical dependencies $E_g(C, T)$ (here C is the concentration of the binary compound) for MCT [40], for ZMT [41]

and for ZCT [3] are used in this method. These dependencies were averaged, taking into account the statistical weight of each dependency as indicated by the component concentration. The corresponding $E_g(T)$ curves are shown in figure 12, where curve 1 represents composition IV and curve 3 represents composition VI. It is obvious that the points of the curves are considerably lower than the points corresponding to the energy gap values obtained by means of MPR (squares in figure 12). These discrepancies are probably caused by the difference in the concentration of the components within those regions where the electron transport occurs and the averaged compound concentration obtained by x-ray microanalysis (the space resolution for these measurements exceeds 1 μm). Unbounded HgTe and ZnTe clusters are formed due to the escape of Hg and Zn atoms out of this region. One can estimate the molar percentages of HgTe and ZnTe constituting the clusters, by fitting the $E_g(x, y, T)$ dependence to the values of the energy gap obtained from the temperature shift of the MPR peaks. In figure 12, the dependence $E_g(T)$ which is calculated for $x' = 0.0775$, $y' = 0.13$ and $x'' = 0.165$, $y'' = 0.10$ is represented as curves 2 and 4, respectively. The solid solution $Zn_{x'}Cd_{y'}Hg_{1-x'-y'}Te$ (curve 2) is obtained from composition IV ($x = 0.08$, $y = 0.11$) by reducing the ZnTe concentration by 1.5% and the HgTe concentration by 2.5%. Analogously, the composition with x'' and y'' is obtained from composition VI by reducing the ZnTe concentration by 2.5% and the HgTe concentration by 3.5%.

Hence, there is agreement between the temperature dependencies of the energy gaps obtained from the temperature shifts of MPRs and those obtained from the empirical dependencies $E_g(x, y, t)$. To obtain the aforementioned agreement, it was necessary to substitute, for the measured concentration of components, a ZnTe concentration reduced by 1.5% and a HgTe concentration reduced by 2.5% for sample IV (2.5% and 3.5% for sample VI, respectively). We believe that it is these materials, i.e. 1.5% of ZnTe and 2.5% of HgTe (sample IV) or 2.5% of ZnTe and 3.5% of HgTe (sample VI), that compose the ZnTe and HgTe clusters.

9. Conclusions

Investigations of the phonon subsystems (by means of Raman scattering) of the complex four-component solid solutions $Zn_xCd_yHg_{1-x-y}Te$ and their interactions with the electron subsystems (by means of MPR) have led to the following conclusions.

(i) The lattice of three cations (Hg, Cd, Zn) with a single common anion (Te) undoubtedly gives rise to three-mode phonon spectra, which correspond to the stochastically homogeneous distribution of cation atoms.

(ii) In reality, crystal stochastic homogeneity can be locally damaged and clusters with anions predominantly surrounded by Zn atoms or Hg atoms can appear; these are ZnTe clusters and HgTe clusters, respectively.

(iii) The electron transport in such a lattice occurs in the channels of high mobility (for example, the ones going round the ZnTe clusters); the electrons interact with the long-range polarization fields of the complete range of long-wavelength longitudinal vibrations (including the ZnTe clusters).

(iv) No less than four kinds of LO phonon participate in the electron–phonon interactions in $Zn_xCd_yHg_{1-x-y}Te$ solid solutions.

(v) Two kinds of MPR on the difference of phonon frequencies (with simultaneous absorption and emission of LO phonons belonging to different sublattices of ZMCT solid solutions) are evident within the range of weak magnetic fields.

(vi) The band-structure parameters obtained from the MPR correspond to that part of the solid-solution crystal lattice where the electron transport occurs; the composition of this part can be to some extent different from the averaged compound concentration.

Acknowledgments

References

[1] Sher A, Chen A-B, Spicer W E and Shih C-K 1985 *J. Vac. Sci. Technol.* A **3** 105
[2] Triboulet R 1988 *J. Cryst. Growth* **86** 79
[3] Bazhenov N L, Andruchiv A M and Ivanov-Omskii V I 1993 *Infrared. Phys.* **34** 357
[4] Rogalski A and Piotrowski J 1988 Intrinsic infrared photodetectors *Prog. Quantum Electron.* **12** 87
[5] Rogalski A 1994 *New Ternary Alloy System for Infrared Detectors* (Bellingham, WA: SPIE)
[6] Andruchiv A M, Gadajev, Ivanov-Omskii V I, Mironov K E, Smirnov V E, Yuldashev S U and Cidil'kovskii E I 1992 *Fiz. Tekh. Poluprov.* **26** 1288
[7] Guculiak L M, Ivanov-Omskii V I, Cypishka D I and Andruchiv A M 1996 *Fiz. Tekh. Poluprov.* **30** 2042
[8] Nicholas R J 1985 *Prog. Quantum Electron.* **10** 1
[9] Polit J, Sheregii E, Andruchiv A and Sydorchuk P 1994 *Die Kunst of Phonons* ed T Paszkiewicz (New York: Plenum) pp 415–418
[10] Andruchiv A M, Ivanov-Omskii V I, Polit J and Sheregii E M 1995 *Acta Phys. Pol.* A **87** 513
[11] Sheregii E M, Polit J, Cebulski J and Andruchiv A M 1995 *Phys. Status Solidi* b **192** 121
[12] Baars J and Sorger F 1972 *Solid State Commun.* **10** 875
[13] Polian A, Le Youllec R and Balkanski M 1976 *Phys. Rev.* B **13** 3558
[14] Kozyrev S P, Vodopyanov L K and Triboulet R 1983 *Solid State Commun.* **45** 383
[15] Sheregii E M and Ugrin Yu O 1992 *Solid State Commun.* **83** 1043
[16] Harada H and Narita S 1971 *J. Phys. Soc. Japan* **30** 1628
[17] Vodopyanov L K, Vinogradov E A, Blinov A M and Rukavishnikov V A 1972 *Sov. Phys.–Solid State* **14** 219
[18] Perkowitz S, Kim L S and Feng Z C 1990 *Phys. Rev.* B **42** 1455
[19] Sheregii E M, Ugrin Yu O, Shuptar D D and Leshko O M 1988 *JETP Lett.* **47** 711
[20] Taylor D W 1988 *Optical Properties of Mixed Crystals (Modern Problems in Condensed Matter Sciences 23)* ed R J Elliott and I P Ipatova (series ed V M Agranovich and A A Maradudin) (Amsterdam: North-Holland) pp 35–131
[21] Sochinski N V, Serrano M D and Diegues E 1995 *J. Appl. Phys.* **77** 2806
[22] Tiong K K, Amirtharaj P M, Parayanthal P and Pollak F H 1984 *Solid State Commun.* **50** 891
[23] Polit J, Sheregii E M, Szczecinska E, Szczecinski J and Ivanov-Omskii V I 1998 *Phys. Status Solidi* b **208** 21
[24] Klingshirn C F 1995 *Semiconductor Optics* (Berlin: Springer)
[25] da Costa V M and Coleman L B 1991 *Phys. Rev.* B **43** 1903
[26] Rowe J M, Niclow R M, Price D L and Zanino K 1974 *Phys. Rev.* B **10** 621
[27] Vegalatos N, Wahne D and King J S 1974 *J. Chem. Phys.* **60** 3613
[28] Aggarwal R L 1972 *Semiconductors and Semimetals* vol 9, ed R K Willardson and A C Beer (New York: Academic) pp 169–85
[29] Pidgeon C R and Brown R N 1966 *Phys. Rev.* **146** 575
[30] Kane O 1957 *J. Phys. Chem Solids* **1** 249
[31] Shantharama L G, Adams A R, Ahmad C N and Nicholas R J 1984 *J. Phys. C: Solid State Phys.* **17** 4429
[32] Pfeffer P and Zawadsky W 1990 *Phys. Rev.* B **41** 1561
[33] Luttinger J M 1956 *Phys. Rev.* **102** 1030
[34] Weiler M H, Aggarwal R L and Lax B 1977 *Phys. Rev.* B **16** 3603
[35] Guldner Y, Rigaux C, Mycielski A and Couder Y 1977 *Phys. Status Solidi* b **81** 615
[36] Guldner Y, Rigaux C, Mycielski A and Couder Y 1977 *Phys. Status Solidi* b **82** 149
[37] Ugrin Yu O, Sheregii E M, Gorbatiuk I M and Rarenko I M 1990 *Fiz. Tverd. Tela* **32** 43

[38] Gelmont B L, Seisyan R P and Efros A L 1982 *Fiz. Tekh. Poluprov.* **16** 776
[39] Gelmont B L, Golubev B G and Ivanov-Omskii V I 1979 *Fiz. Tverd. Tela* **21** 1084
[40] Weiler M H 1981 *Semiconductors and Semimetals* vol 16, ed R K Willardson and A C Beer (New York: Academic) pp 119–91
[41] Toulous B, Granger R, Rolland S and Triboulet R 1987 *J. Phys. C: Solid State Phys.* **48** 247